Responsive Liquid Crystal Micro Actuators for Microrobotic Applications

2019 CNF REU Intern: Anna Alvarez

2019 CNF REU Intern Affiliation:
Mechanical Engineering, University of Illinois at Urbana Champaign

CNF Project: 2019 Cornell NanoScale Science & Technology Facility Research Experiences for Undergraduates Program

CNF REU Principal Investigator(s): Prof. Itai Cohen, Department of Physics, Cornell University

CNF REU Mentor(s): Qingkun Liu, Department of Physics, Cornell University

Primary Source of CNF REU Funding: National Science Foundation via the National Nanotechnology Coordinated Infrastructure (NNCI) Grant No. NNCI-1542081

Contact: itai.cohen@cornell.edu, ql59@cornell.edu

Website: http://cnf.cornell.edu/education/reu/2019

Primary CNF Tools Used: ABM contact aligner, MVD 100, Oxford 81, Unaxis 770 deep Si etcher, Heidelberg mask writer - DWL2000

Abstract:

Multifunctional micro-sized soft robotics are poised to revolutionize drug delivery, surgical operation and many other biomedical applications. However, building such microrobots with a variety of functionalities is challenging due to the lack of fabrication technologies for responsive materials at the microscale. In this research, we developed a scalable microfabrication technology to build light and thermal activated microrobots using liquid crystal (LC) polymers, which are known for their facile response to relatively weak stimuli. First, an ultraviolet light curable precursor containing LC oligomers was developed, allowing for patterning of the LC microrobots via photolithography. Second, fluoroctyl-trichlorosilane-coated silicon microgrooves were used to establish unidirectional alignment in LC microactuators. Finally, heat was applied to confirm the LC microactuators could properly contract along the alignment direction as expected when experiencing a phase transition from the LC to its isotropic phase. These LC microactuators could further bend as hinges if an athermal photoresist was patterned on top, allowing 2D patterned films to fold into 3D objects. Fabricating these LC-based responsive microrobots in a scalable way will provide a powerful platform for dynamically reconfigurable micro-sized origami-robots.

Summary of Research:

The field of microrobotics presents a promising future for advancements in sensing, surgery, and drug delivery. However, current microrobots are only capable of performing simple functions, such as self-propulsion or particle encapsulation [1]. In order to evolve into multifunctional, controllable devices, it is necessary to develop a new actuation system. In this work, we propose to use of photopatternable responsive liquid crystal (LC) polymer to fabricate micro-scale devices from.

The initial challenge of this project was to develop an ultraviolet (UV) curable LC precursor compatible with photolithography technology. The precursor contained a photoinitiator, a 3:1 molar ratio of LC diacrylate to butylamine, and chloroform as the solvent. To test precursor performance, the substance was spin coated at 1000 rpm, yielding a thickness of 2.5 μm. Exposure to UV light in the ABM contact aligner excited the photoinitiator and a postbake at 90°C released free radicals to complete polymerization [2]. From successful samples, features 50 μm and smaller can be observed. However, photopatterning the LC polymer with no initial alignment results in a speckled image when viewed through crossed polarizers (Figure 1). Given no set direction to follow, the LC mesogens align themselves in random orientations.

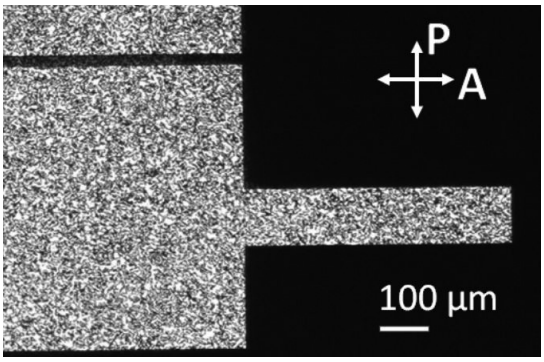

Figure 1: A well-developed LC pattern viewed between crossed polarizers (A and P).

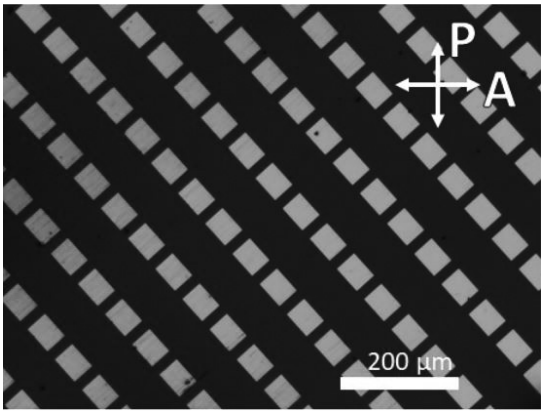

Figure 2: Well aligned LC patterns oriented 45° relative to the polarizers.

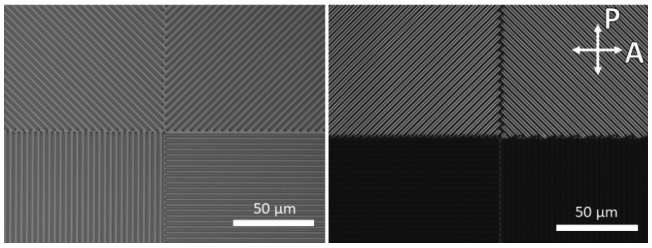

Figure 3: (a) 1.5 µm wide and 1.4 µm deep Si grooves with four orientations. (b) Aligned LC on top of etched Si grooves. Birefringent materials appear brightest when aligned 45° relative to the polarizer and darkest when 0° or 90° relative to the polarizer. The black lower half of the image suggests near perfect alignment.

For an LC polymer actuator to work, it is crucial that the mesogens display predesigned alignment. LC polymers will expand along the direction of average molecular alignment and contract in the perpendicular when transitioning from isotropic to LC phase. Altering the surface architecture was accomplished through two methods. In the first, the substrate was spin-coated with polyimide PI-2555 and physically rubbed with a velvet cloth after a 30 minute-long bake at 170°C. The LC polymer achieved planar anchoring and aligned along the rubbing orientation. This method proved to be a reliable technique and resulted in few defects (Figure 2). While suitable for aligning simple patterns, such as cantilever beams, it is unable to align the LC polymer in differing orientations. Fabricating a micro robot that can actuate hinges in various directions requires a more versatile micropatterning technique. In the second method, fluoroctyl-trichlorosilane-coated silicon microgrooves, 1.5 µm wide and 1.4 µm deep, were etched to establish an arbitrary alignment (Figure 3a). The LC once again can be aligned planarly along the groove geometry, as visible in Figure 3b.

The final challenge of this work was inducing actuation of the aligned LC polymer in response to heat. Patterned cantilevers were released from the substrate during development in IPA and exposed to 90°C while still submerged in the solution. LC can only expand and

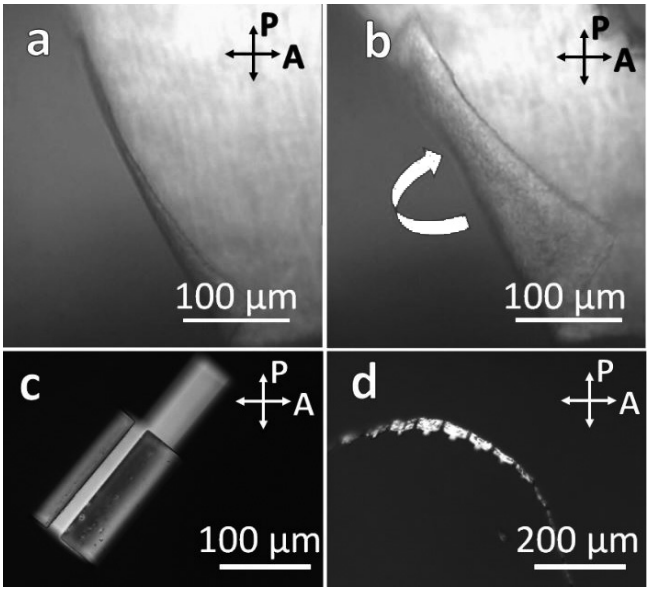

Figure 4: (a) Cantilever edge at 60°C. (b) Cantilever edge at 90°C. (c) A curled cantilever pattern. (d) A connected chain of released cantilevers.

contract in the 2D plane when experiencing a phase transition. However, the combination of athermal polymer PI-2555 and LC coating proved to be an efficient bimorph, allowing the 2D patterned films to fold into 3D shapes (Figure 4a,b) in response to the elevated temperature. Successful actuations thus far (Figure 4c) have a measured radius of curvature of 25 µm. To further improve the quality of the LC-patterned films, an oxygen plasma etch was required to remove fringes of excess polymer before IPA development. This is to prevent a chain of adhering cantilevers (Figure 4d). Continued work will focus on doping the LC precursor with a photoresponsive dye to induce actuation via light exposure.

The use of responsive LC films is a promising platform for microrobotic actuation. Not only has this work shown it is possible to fabricate LC films with available nanofabrication technology, but it is possible to align the polymers through patternable microgrooves as well. Future development of these actuators may lead to new fields of reconfigurable origami-based microrobots.

Acknowledgements:

I would like to thank Professor Itai Cohen, Qingkun Liu, and the CNF staff for their support this summer. This work was carried out as part of the 2019 CNF REU Program and supported by the National Science Foundation (Grant No. NNCI-1542081).

References:

[1] M. Medina-Sánchez, V. Magdanz, M. Guix, V.M. Fomin, O.G. Schmidt, O. G. Adv. Funct. Mater. 28, 1707228, 2018.

[2] T. H. Ware, T. J. White, Polym. Chem. 6, 4835, 2015.

ALD for Membranes, Metamaterials, and Mechanisms

CNF Project Number: 900-00

Principal Investigator(s): Paul L. McEuen[1,2], Itai Cohen[1,2]

User(s): Tanner Pearson[3], Kyle Dorsey[3], Edward Esposito[1], Sierra Russell[4], Baris Bircan[3]

Affiliation(s): 1. Laboratory of Atomic and Solid State Physics, Cornell University; 2. Kavli Institute for Nanoscale Science, Cornell University; 3. School of Applied and Engineering Physics, Cornell University; 4. College of Nanoscale Sciences, SUNY Polytechnic Institute

Rrimary Source(s) of Research Funding: NSF grant DMR-1435829, Air Force Office of Scientific Research (AFSOR) multidisciplinary research program of the university research initiative grant FA2386-13-1-4118, Cornell Center for Materials Research (CCMR) through NSF MRSEC program (DMR-1719875), ARO grant W911NF-18-1-0032, National Science Foundation (NSF) Major Research Instrumentation Award DMR-1429155, NNCI Grant No. NNCI-1542081, and the Kavli Institute at Cornell for Nanoscale Science

Contact: plm23@cornell.edu, itai.cohen@cornell.edu, tgp34@cornell.edu, kjd96@cornell.edu, epe3@cornell.edu, srussell@sunypoly.edu, bb625@cornell.edu

Primary CNF Tools Used: Oxford FlexAL ALD, Arradiance ALD, Autostep AS200 i-line stepper, CVC e-beam evaporators, Oxford 81/82 etchers, PT770 and PT740 etchers, Anatech Asher, Zeiss SEMs, Veeco AFM, Tencor P7 profilometer, Filmetrics UV, Woollam ellipsometer, DISCO dicing saw, Heidelberg DWL2000, AJA sputterer

Abstract:

Bending and folding techniques such as origami and kirigami enable the scale-invariant design of three-dimensional structures, metamaterials, and robots from two-dimensional starting materials. Such techniques have been used in everything from deployable spacecraft solar panel arrays [1], soft robots [2], and microelectromechanical systems (MEMS) [3]. These design principles are especially valuable for small systems because most micro- and nanofabrication involves lithographic patterning of planar materials. Ultra-thin films of inorganic materials serve as an ideal substrate for the fabrication of flexible microsystems because they possess high intrinsic strength, are not susceptible to plasticity, and are easily integrated into microfabrication processes [4]. In recent work, we employed atomic layer deposition (ALD) to synthesize films down to 2 nm thicknesses to create membranes, metamaterials, and machines with micron scale dimensions [5]. In this thickness limit, ALD films behave elastically and can be fabricated with femtojoule-scale bending stiffnesses. Further, ALD membranes are utilized to design micron-scale mechanical metamaterials and magnetically actuated three-dimensional devices. These results establish thin ALD films as a scalable basis for micron-scale actuators and robotics.

Summary of Research:

ALD is an ideal technique for scaling mechanical systems to micron-scale dimensions. We have developed an entire fabrication strategy around ALD, including lithography, etching, release, and integration. ALD films are grown conformally on a sacrificial layer of aluminum, as shown schematically in Figure 1. The devices consist of lithographically patterned regions of ALD membranes and thicker panels of other materials that provide rigid structure and additional functions such as mirrors or magnets. The devices are fabricated at wafer scales at yields exceeding 90%. The wafer is diced and devices are released by immersing in dilute base, followed by rinsing in water. Upon release, all experiments are carried out in aqueous environments, often with added surfactant, to avoid stiction of the free membranes.

We investigated the mechanical properties of these films by measuring the bending stiffness of over 60 magnetically actuated glass hinges. Ferromagnets with a saturated in-plane moments are patterned on panels at the ends of the hinges. The panels are deflected when we apply an out-of-plane magnetic field B (Figure 2a). Figure 2b shows the measured hinge deflection angles for ALD films of two different thicknesses, 5 and 8 nm, as a function of the magnetic field B. The hinges are deflected reversibly with no observable hysteresis. By equating the magnetic torque to the opposing mechanical torque due to the bending stiffness of the film, we deduce a linear relationship between the deflection angle and the applied field. The bending stiffness of each individual hinge can be extracted from the slope of this relationship.

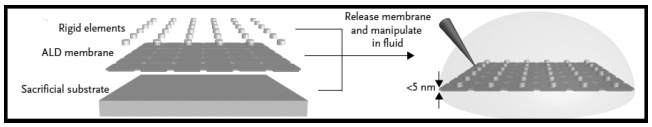

Figure 1: Schematic of the fabrication and release processes.

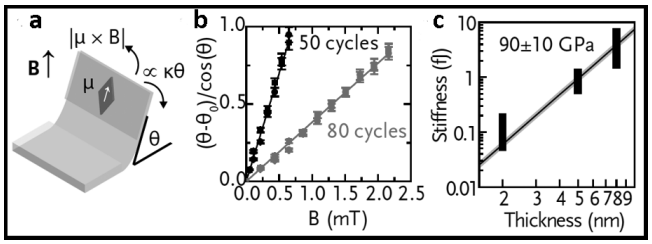

Figure 2: Mechanical characterization of ALD glass hinges.

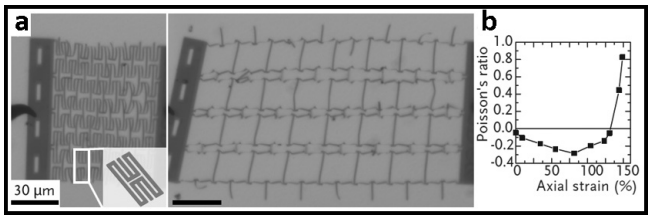

Figure 3: Auxetic mechanical metamaterial made of ALD Pt.

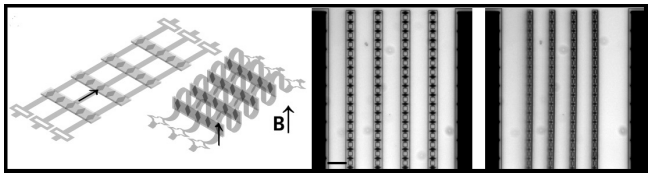

Figure 4: Magnetically actuated muscle-like device.

Scaling the thickness from 2 nm to 8 nm, we find bending stiffnesses spanning nearly two orders of magnitude in the femtojoule range (Figure 2c). We extract the Young's modulus of ALD glass from the fit in Figure 2c, finding Y = 90 ± 10 GPa. This value is comparable to values for bulk material (70-80 GPa), indicating that even at 2 nm thickness, the films behave mechanically similar to macroscopic counterparts.

We additionally use ALD membranes to fabricate mechanical metamaterials through in-plane and out-of-plane patterning. The sheet can become stretchable by cutting patterns that allow parts of the sheet to bend/buckle out of its fabrication plane. A metamaterial with a negative Poisson's ratio, also known as an auxetic, is shown in Figure 3a. This material is patterned from 5 nm-thick sheet of ALD platinum. Under application of an axial strain, the sheet expands in the transverse direction, yielding a negative Poisson's ratio (Figure 3b).

These ultra-thin materials can also be used for micron-scale actuators and machines that function with exquisitely small forces and torques. The device shown in Figure 4 is a magnetically actuated mechanism that contracts to bear a load. The magnetic panels are attached to linear springs. Upon application of an external field, the panels rotate out of the plane and move laterally closer to each other while applying a load on the springs in a fashion analogous to a muscle.

The mechanical properties and fabrication protocols for ALD membranes and metamaterials facilitates their potential application in very sophisticated micromechanical systems. For example, the low processing temperatures and fabrication compatibility enable ALD actuators to be added to silicon-based integrated circuits for smart microsystems and machinery. In addition, the diverse materials palate offered by ALD enables bimorph actuators of dissimilar materials while still maintaining a low bending stiffness for the film stack. These actuators can be leveraged to create self-assembled and environmentally responsive three-dimensional structures and actuators. An additional benefit of ultra-thin versions of bulk materials is that the surface chemistry of many ALD films is well-studied. This enables chemical functionalization and patterning, enabling the coupling between chemical sensitivity and mechanical responsivity. Combination of these capabilities may be used for sensors, self-assembled devices, optical devices, and microscale robotic systems.

References:

[1] S. A. Zirbel, B. P. Trease, M. W. Thomson, R. J. Lang, S. P. Magleby, L. H. Howell in Micro- and Nanotechnology Sensors, Systems, and Applications VII, Vol. 9467, International Society for Optics and Photonics, 2015, pp. 94671C-1.

[2] D. Rus, M. T. Tolley, Nature 2015, 521, 467.

[3] N. T. Eigenfeld, J. M. Gray, J. J. Brown, G. D. Skidmore, S. M. George, V. M. Bright, Adv. Mater. 2014, 26, 3962.

[4] M. Z. Miskin, K. J. Dorsey, B. Bircan, Y. Han, D. A. Muller, P. L. McEuen, I. Cohen, Proc. Natl. Acad. Sci. U.S.A. 2018, 113, 466.

[5] K. J. Dorsey, T. G. Pearson, E. Esposito, S. Russell, B. Bircan, Y. Han, M. Z. Miskin, D. A. Muller, I. Cohen, P. L. McEuen, Adv. Mater., doi: 10.1002/adma.201901944, 2019.

Localized Microfluidic Actuation and Mixing Using Planar Fresnel Type Gigahertz Ultrasonic Transducer

CNF Project Number: 1121-03

Principal Investigator(s): Amit Lal

User(s): Adarsh Ravi

Affiliation(s): Electrical and Computer Engineering, Cornell University

Primary Source(s) of Research Funding: Intelligence Advanced Research Projects Activity (IARPA) - Trusted Integrated Chips (TIC) program, and National Science Foundation (NSF) - Emerging Frontiers in Research and Innovation (EFRI) program

Contact: amit.lal@cornell.edu, ar2256@cornell.edu

Website: http://sonicmems.ece.cornell.edu/

Primary CNF Tools Used: Heidelberg mask writer - DWL2000, Westbond 7400A ultrasonic wire bonder, ABM contact aligner, SU-8 Hotplates, YES Polyimide Bake Oven, Optical Microscopes, CorSolutions microfluidic probe station, Harrick plasma generator, high-temperature PDMS curing oven, low-temp PDMS vacuum oven, Tencor P7 profilometer

Abstract:

We report on an AlN-based gigahertz (GHz) frequency ultrasonic transducer for microparticle actuation and microfluidic mixing. The device uses focusing transducers placed in a Fresnel lens configuration, which generates bulk acoustic waves through the silicon substrate adding in phase at the focus. The device is planar and is fabricated with a CMOS compatible process, with no thin-film release steps. Peak displacement of 250 pm was achieved at the focus with 5 V_p, 1.06 GHz RF input. Owing to high absorption at gigahertz, vortices with streaming velocities > 2.6 mm/s in water were generated, and localized mixing of blue dye and water with 90% efficiency was observed.

Introduction:

Among the contactless microparticle manipulation mechanisms, optical and acoustic techniques are the most common. The laser based optical technique can produce a few pico-Newton of trapping force, but cannot control larger biological objects and operate in a medium of high optical opacity [1,4]. On the other hand, acoustic devices can be more easily integrated with the microfluidic channel and have been shown to handle biological particles better because of longer wavelengths and higher forces [1-3].

Efficient and rapid mixing of laminar fluid flows is critical for several microfluidic applications such as drug screening, chemical synthesis, genetic analysis, protein folding studies, etc. [3-5]. Traditional macroscopic fluidic mixing strategies employing long channels, mechanical or magnetic stirring elements become impractical for microscale mixing. Furthermore, as microfluidic flow lies in the laminar regime, mixing is dominated by diffusion, which is slow and prevents mixing in channel lengths compatible with microfluidic chip dimensions [2,4].

To improve the mixing time and homogeneity, various approaches have been employed. These approaches can be classified into passive and active mixing based on the absence or presence of an external energy source. Active mixers generally outperform the passive counterparts with respect to mixing time, efficiency, and required channel length. Active microfluidic mixers employing external electrical, thermal, magnetic or acoustic energy sources have been reported [5]. However, acoustic mixers are advantageous as they perform contactless fluidic mixing without any restriction on the electrical properties of the fluids.

Acoustic mixers perturb the streamlined flow in the microfluidic channel by employing bulk acoustic wave (BAW), surface acoustic wave (SAW) or membrane transducers. For efficient mixing, strong acoustic streaming forces are required. The body force that generates streaming vortices at the edges of the acoustic fields in fluids scales as $F_B \propto f^4$, where f is the frequency. As a result, much interest is being showed in developing ultra-high frequency SAW and BAW based microfluidic actuators and mixers [4,5]. However, most of these actuators reported thus far require > 10 V_p drive voltage and are fabricated using non-CMOS compatible materials such as ZnO, $LiNbO_3$, $LiTaO_3$ or PZT [4].

Furthermore, in most of these devices, the fluid is placed on the same side of these transducers. This then forces considerable chip area dedicated to isolate electrical

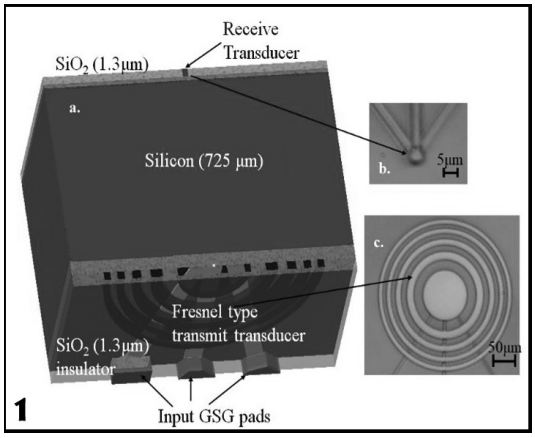

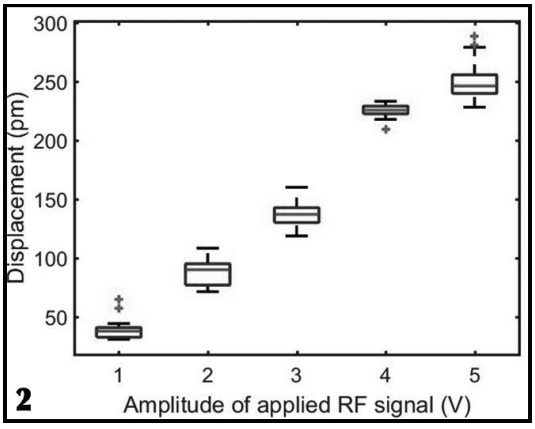

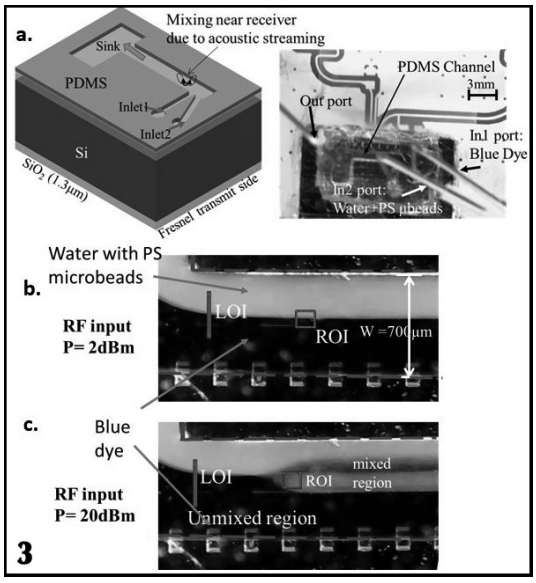

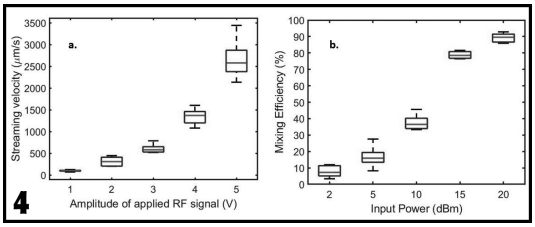

interconnects from the fluidic sample. These factors can result in increased device area, expense of fabrication, and electronics complexity in the generation and amplification of high voltages at ultra-high frequencies.

Summary of Research:

The acoustofluidic micro-mixer and actuator presented here uses gigahertz focused ultrasonic beam to create localized streaming vortices in the microchannel. The device is fabricated without any thin-film release steps, using CMOS compatible materials like aluminum nitride solidly mounted to silicon substrate. Further, the placement of the transducers on the opposite side of fluidics enable easier integration of distributed CMOS electronics with AlN transducers on one side, and the fluidic system on the opposite side. The cross-sectional sketch of the simplified GHz transducer stack with planar FZP shaped AlN transducer on the transmit side and a small circular AlN transducer on the receive side is shown in Figure 1. AlN in the regions without transduction are not shown here for simplicity. Figure 2 shows the peak displacements at the point of focus for different RF drive voltages.

A PDMS microfluidic channel with two inlet ports and an outlet port was fabricated using standard soft lithography process. The molds for the PDMS channel were made using 325 μm thick SU-8-100 photoresist spun onto a clean silicon wafer. The photo resist was patterned using UV contact lithography to make a 700 μm wide channel. PDMS resulting by mixing Sylgard-184 elastomer base and curing agent in the mass ratio 10:1 was poured onto the silicon wafer with SU-8 master. The cured PDMS stamp was then peeled off from the silicon wafer to make a microfluidic channel. The surfaces of the PDMS channel and the AlN-Si transducer stack were modified using a room temperature plasma cleaner before bonding. The image of the PDMS channel bonded onto the AlN-Si transducer substrate is shown in Figure 3. Figure 4 shows the results from the mixing activity and the streaming velocities for different drive voltages.

References:

[1] C. Lee, et al., "Single microparticle manipulation by an ultrasound beam," IEEE International Ultrasonics Symposium, 849-852, 2010.

[2] B. W. Drinkwater, "Dynamic-field devices for the ultrasonic manipulation of microparticles," Lab Chip, 16, 2360, 2016.

[3] A. Sarvazyan, et al., "Stirring and mixing of liquids using acoustic radiation force," The Journal of the Acoustic Society of America 125, 3548, 2009.

[4] A. Ravi, et al., "CMOS compatible GHz ultrasonic Fresnel microfluidic actuator," Technical Digest of the 2018 Solid-State Sensor and Actuator Workshop, Hilton Head Isl., SC, 2018.

[5] A. Ravi, et al., "Localized Microfluidic mixer using planar Fresnel type GHz ultrasonic transducer," IEEE International Ultrasonic Symposium, Japan, 2018.

Figure 1: *Cross sectional schematic of the AlN-Si stack (a) and images of the Fresnel lens transmit (c) and circular receive (b) transducers post fabrication.* **Figure 2:** *Plot of surface displacement at the point of focus against different applied voltages.* **Figure 3:** *a. image of the GHz acoustofluidic micro-mixer after bonding. Image captures showing: negligible mixing activity near the receive transducer when RF input power is 2 dBm (a) and localized mixing when RF input power is 20 dBm (c) (LOI - Line of interest; ROI - region of interest for mixing efficiency calculation).* **Figure 4:** *a. Box plot of streaming velocity versus applied voltage. b. Box plot of mixing efficiency vs. applied RF input.*

N-Z Power NEMS Electrostatic RF Wakeup Receiver with Pt Contact

CNF Project Number: 1262-04

Principal Investigator(s): Amit Lal

User(s): Alexander Ruyack

Affiliation(s): Electrical and Computer Engineering, Cornell University

Primary Source(s) of Research Funding: Defense Advanced Research Projects Agency (DARPA) project: Near Zero Power RF and Sensor Operations (N-ZERO)

Contact: amit.lal@cornell.edu, arr68@cornell.edu

Primary CNF Tools Used: ASML 300C DUV stepper, Heidelberg mask writer DWL2000, Gamma automatic coat-develop tool, Zeiss Ultra SEM, Zeiss Supra SEM, Oxford 81, 82 etchers, Oxford 100 etcher, AJA ion mill, Hamatech hot piranha, Primaxx Vapor HF etcher, Plasma-Therm deep Si etcher, Uniaxis 770 deep Si etcher, DISCO dicing saw, wire bonder, Aura 100, Zygo, furnaces, ResMap, Nanostrip Bath

Abstract:

This work reports a nanoelectromechanical systems (NEMS) electrostatic RF switch usable as a near-zero power wake-up receiver capable of detection sensitivity reaching -25 dBm off resonance with sub-pW passive power consumption at less than 1.5V DC operation. The switch utilizes a multielectrode design allowing for a mechanical contact gap to be held just outside thermal oscillations and the radio frequency (RF) input to physically close the switch. This allows for operation away from pull-in and improves RF sensitivity. A focused ion beam (FIB) patterned platinum-platinum contact point enables the low DC bias requirement and improves contact resistance and longevity. The potential for on-resonance operation provides a pathway forward for improved RF sensitivity in the future.

Introduction:

With the advent of RF connectivity between sensors and the subsequent proliferation of wireless sensor nodes, power consumption and battery management of distributed sensor networks has become a bottleneck for widespread implementation. With applications spanning smart cities, agricultural monitoring and military scenarios, replacing batteries for increasing size sensor arrays is becoming costly, time consuming with significant downtimes, and potentially dangerous for reaching sensors in remote locations. Beyond advancements in battery technology and power reduction of active components, asleep-yet-aware sensors provide a means for reducing power consumption and significantly extending sensor node lifetime. These sensors work by operating in a low power, or near zero power, mode (typically comparable to battery leakage) but remain triggerable by signals of interest, turning on higher power electronics (like communications or signal processing) only when this signal is perceived and only for the duration required. For sensing applications in which signals of interest are infrequent, this modality can improve sensor operational lifetime by orders of magnitude.

These schemes have been implemented in a wide variety of physical sensors including accelerometers, microphones and magnetic field sensors, among others [1,2]. Near-zero power RF wake-up sensors have been widely developed using CMOS, but state of the art has struggled to push powers lower than single digit nW at -60 to -70 dBm RF sensitivity [3,4]. MEMS based RF wake-up sensors are much less have the distinct advantage of extremely low power draw but are much less common due to complications in design and fabrication limiting their sensitivity [5,6].

In order to maintain this lower power but improve RF sensitivity, we have improved upon a near-KT lateral NEMS switch that showed 300 μV switching at 50V DC bias [7]. This is accomplished by utilizing a multielectrode design to enable device switching without pull-in. Additional fabrication changes including, but not limited to, a compliant contact and FIB post-processing device contact areas, have also been implemented to reduce the DC bias requirement and improve device longevity.

Summary of Research:

The switch is operated primarily by a set of DC bias electrodes and a single RF electrode, all of which electrostatically actuate a released shuttle and move it towards a contact electrode biased with a small voltage. The switch also contains a reset electrode that applies an electrostatic force in the opposite direction to the DC and RF electrodes, ensuring a means of un-sticking the switch if necessary. Figure 1 shows the general layout and the relevant switch components.

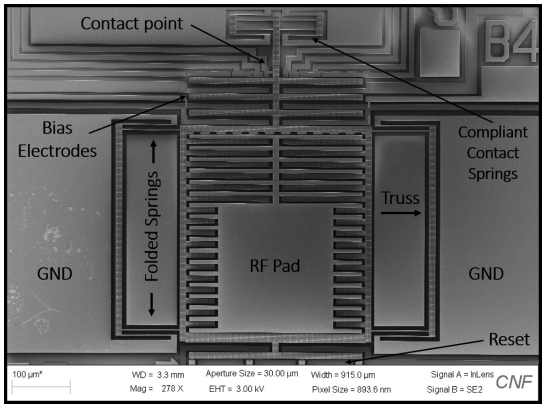

Figure 1: SEM micrograph of NEMS switch from above showing important electrical contacts and features.

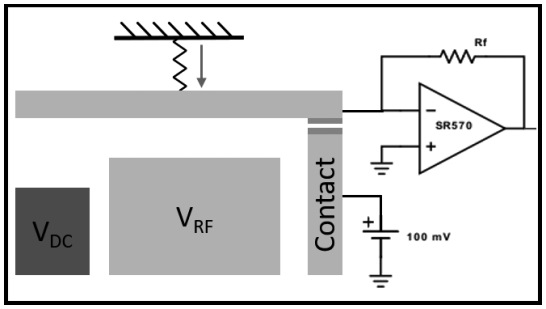

Figure 3: Simplified schematic of switch components showing biasing electrodes and TIA for detection.

Device fabrication follows a typical one mask SOI micromachining process with a vapor HF release. A full description of the device fabrication is available in last year's CNF technical report or [8]. Figure 2 shows an SEM image of the device contact area modified with Pt from a FIB process.

For operation, the switch is first pre-biased using the DC electrodes to bring the shuttle nearly into contact. The device is designed such that pull-in is not reached during this step. After pre-biasing, the RF wake-up signal is then applied to the RF electrode, which closes the switch the rest of the way. A TIA is used to read out a voltage when the switch closes. Figure 3 depicts a simplified schematic of the switch after DC pre-biasing and awaiting an RF input.

Testing is accomplished with a custom vacuum probe station with Python code managing a control loop running a MAXIM 5318 18-bit DAC, SR570 TIA and R&S SMC100A RF source. RF Probability of Detection (PoD) and False Alarm testing is accomplished using this automated code, described in [9]. Figure 4 shows a successful PoD test with -25 dBm sensitivity. Typical power consumption is 0.2 pW with a DC bias requirement of less than 1.5V. Ongoing work aims to operate the switch on resonance by modulating the RF signal at the device resonance.

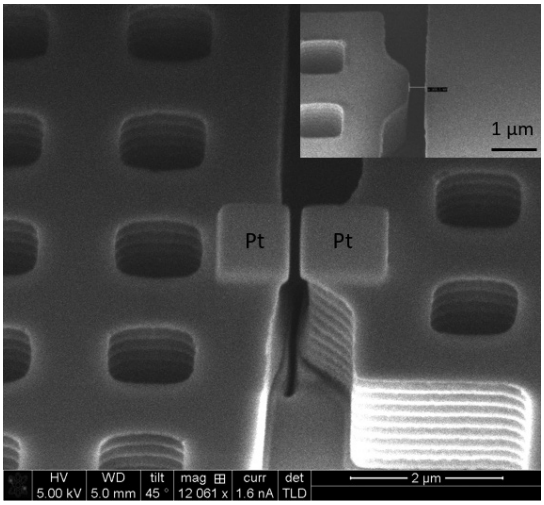

Figure 2: SEM micrograph of switch contact after Pt deposition using FIB.

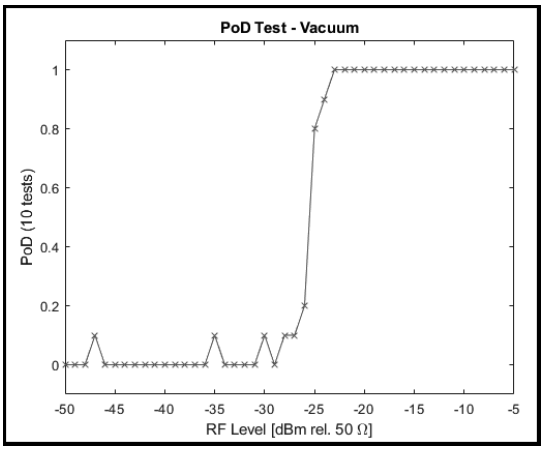

Figure 4: Probability of detection test showing 100% detection (out of 10 tests) for RF amplitudes of -25 dBm and greater.

References:

[1] V. Pinrod, et al., "PZT lateral bimorph-based sensor cuboid for near zero power sensor nodes," IEEE Sensors, 2017.

[2] S. Gupta, et al., "Vibration powered RF-transponder for sensing low frequency motion events," PowerMEMS, 2016.

[3] S. Bdiri, et al., "An 868 MHz 7.5 µW wake-up receiver with 0.60 dBm sensitivity," J. Sens. Sens. Syst., vol. 5, pp. 433-46, 2016.

[4] P. Wang, et al., "A near-zero-power wake-up receiver achieving 0.69-dBm Sensitivity," IEEE Solid-State Circuits, vol. 53, no. 6, pp. 1640-52, 2018.

[5] T. Wu, et al., "Design and Fabrication of AlN RF MEMS Switch for Near-Zero Power RF Wake-Up Receivers," IEEE Sensors, 2017.

[6] W. Vitale, et al., "RF MEMS power sensors for ultra-low power wake-up circuit applications," IEEE ESSDERC, 2013.

[7] K. Amponsah, et al., "Near-kT switching-energy lateral NEMS switch," IEEE NEMS, 2010.

[8] A. Ruyack, et al., "NEMS Electrostatic RF Wakeup Switch with Pt FIB Contact," PowerMEMS, 2018.

[9] A. Ruyack, et al., "NEMS Electrostatic Resonant Near-Zero Power Resistive Contact RF Wake-up Switch with Pt FIB Contact," IEEE MEMS, 2019.

Boiling Heat Transfer Enhancement by Coupling Nanoscale Evaporation in Buried Nanochannels

CNF Project Number: 2123-12

Principal Investigator(s): Shalabh C. Maroo

User(s): An Zou, Sidharth P. Raut, Manish Gupta

Affiliation(s): Department of Mechanical and Aerospace Engineering, Syracuse University, Syracuse, NY 13244

Primary Source(s) of Research Funding: National Science Foundation Career Award NO. 1454450

Contact: scmaroo@syr.edu, azou@syr.edu, spraut@syr.edu, magupta@syr.edu

Website: http://maroo.syr.edu

Primary CNF Tools Used: Heidelberg mask writer DWL 2000, manual photoresist spinner, GAC auto stepper, YES image reversal oven, ABM contact aligner, SÜSS MA6-BA6 contact aligner, e-beam evaporator, Oxford PECVD, GSI PECVD, Glen 1000 Plasma, Anatech resist strip, Oxford 81/82 etcher, optical microscope, scanning electron microscope, atomic force microscope

Abstract:

We explicitly coupled pool boiling with nanoscale evaporation by using buried nanochannels to enhance boiling critical heat flux (CHF) by ~105%. This enhancement is attributed to the formation of extra menisci and contact line in nanochannels. The work reported here is part of a journal article which is currently under review.

Summary of Research:

Boiling and evaporation are two distinct forms of liquid-to-vapor phase change, which is an efficient mechanism to move heat from a solid surface. Boiling has been used in a multitude of residential and industrial applications such as refrigerators, heat exchangers, boilers, etc. However, pool boiling is limited by occurrence of critical heat flux (CHF), the maximum stable heat flux a system can be operated at. Heat flux higher than CHF can irreversibly damage the surface due to a sudden and dramatic temperature increase. CHF occurs when liquid fails to quickly rewet the surface creating dry regions for extended periods of time, with typical values of ~ 80 W/cm^2 for water on silicon dioxide (SiO_2) surface. On the other hand, nanoscale evaporation has recently [1] been shown the capability to remove transient heat flux ~ 8000 W/cm^2 for the same water-silicon dioxide combination over a very short time span in a single 2D nanochannel.

In this work, we combine these two techniques of pool boiling and nanoscale evaporation to increase CHF of pool boiling. The coupling is attained by creating buried 1D nanochannels underneath the surface where wicking in the channels maintains the surface wet, and creates additional evaporating menisci. Thus, nanoscale evaporation occurs in channels and pores, while boiling happens on the surface above.

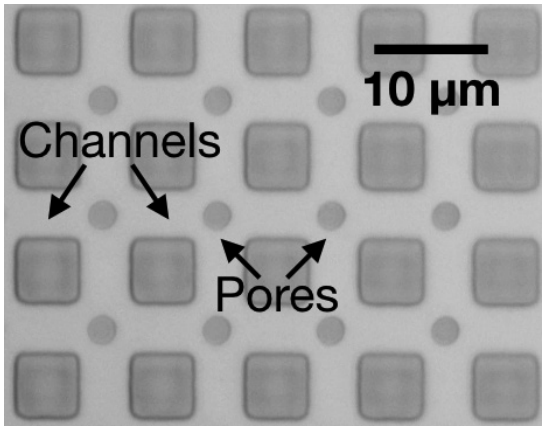

Figure 1: Optical microscope image of the sample with buried nanochannels.

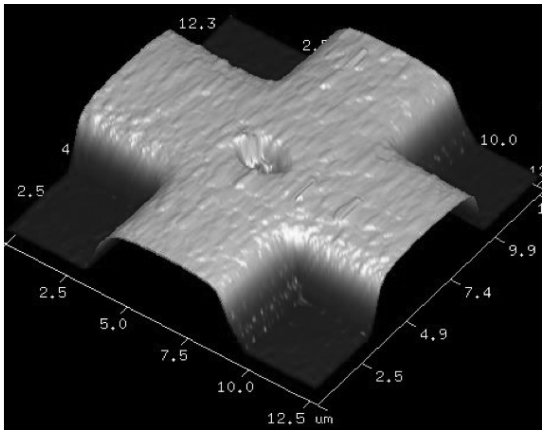

Figure 2: Atomic force microscope (AFM) image of the profile of channels and pores.

The buried cross-connected nanochannels were fabricated on a Si substrate by etching patterned sacrificial metal layers buried under a 300 nm thick SiO_2 film from plasma enhanced chemical vapor deposition (PECVD). The channel geometry was determined by the pattern of sacrificial layers, which was attained by a lift-off process. The cross-connected channels, made from two sets of channels perpendicular to each other, allow for ease of liquid exchange inside the channels. Further, at each intersect of the channels, a 2-μm pore was fabricated allowing liquid present above the surface to flow into the channels. Figure 1 shows an image of these nanochannels (width: 5 μm, spacing: 5 μm, height: 728 nm) from optical microscope. Due to the conformal deposition of PECVD SiO_2, trenches of depth same as channel height formed on the top surface between adjacent channels, Figure 2 shows an atomic force microscope (AFM) image of the surface.

The pool boiling experiments were conducted at atmospheric pressure under saturated conditions using deionized (DI) water. The experiment setup consists of a polycarbonate water bath and a thermal insulated copper block. Five cartridge heaters are embedded in the copper block allowing for a maximum power input of 1250 W (heat flux of 1250 W/cm^2). The heat input to the copper block is controlled with a variable alternating current (AC) to AC transformer. Four equally spaced K-type thermocouples are inserted into the center axis of the copper block to measure the temperature gradient. In water bath, four immersion heaters and a resistance temperature detector (RTD) is used to maintain bulk water at its saturated temperature. In experiments, the sample with buried nanochannels was bonded on the top of the copper block using solder paste to ensure good attachment with minimal thermal contact resistance.

The sample was immersed in a pool of DI water, which was degassed by boiling it for 30 minutes and maintain its temperature at 97-100°C for another 30 minutes. Boiling on sample was achieved by increasing the output voltage of the variable transformer. To obtain the boiling curve, the output of the variable transformer was increased in small increments. The temperature readings were recorded after reaching steady state, which is determined by the criterion that the temperature changes from all thermocouples were less than 0.5°C over one minute. The steady state was reached usually in 10-15 minutes after changing the output power. CHF was obtained when an incremental increase of power supplied resulted in dramatic increase of surface temperature, and its value was taken as the last stable heat flux recorded during experiments. The heat flux was obtained from measured temperature gradient using Fourier's law; while the surface temperature was obtained from the reading from the thermocouple closest to the top surface, also using Fourier's law. ~ 105% CHF enhancement was obtained with an absolute value of 177.40 ± 2.43 W/cm^2.

This enhancement is attributed to nanoscale evaporation from additional menisci inside the nanochannels formed by passive wicking of liquid. This CHF value is in good agreement (within 5% error) to the CHF model, which predicts CHF enhancement when surface force gets augmented due to elongated and/or additional contact line.

In summary, we achieved ~ 105% pool boiling CHF enhancement by explicitly coupling boiling with nanoscale evaporation using nanochannels. This enhancement is mainly contributed by the additional menisci and contact line created by the wicking flow in the nanochannels. The obtained boiling enhancement can be increased by optimizing the nanochannel geometry as well as potentially using 2D nanochannels.

References:

[1] Y. Li, M.A. Alibakhshi, Y. Zhao, and C. Duan, "Exploring ultimate water capillary evaporation in nanoscale conduits," Nano Letters, vol. 17, pp. 4813-4819, 2017.

Fabrication of AlN HBAR Devices for Spin Manipulation of Diamond NV Centers

CNF Project Number: 2126-12

Principal Investigator(s): Gregory Fuchs[1]

User(s): Johnathan Kuan[2], Huiyao Chen[3]

Affiliation(s): 1. Applied and Engineering Physics, 2. Department of Physics, 3. Department of Physics; Cornell University

Primary Source(s) of Research Funding: DARPA-Driven and Nonequilibrium Quantum Systems (DRINQs)

Contact: gdf9@cornell.edu, jk2788@cornell.edu, hc846@cornell.edu

Website: http://fuchs.research.engineering.cornell.edu

Primary CNF Tools Used: AJA sputter, OEM Endeavor M1, GCA 5X stepper, Westbond 7400A ultrasonic wire bonder

Abstract:

Previous work with nitrogen-vacancy (NV) centers in diamond have demonstrated coupling between the NV spins and strain. Harmonic strain can be introduced into diamond lattice with transducers such as high-overtone bulk acoustic resonators (HBAR), which introduce a stress wave into the diamond. This strain can be used to coherently control the NV center spins. We describe our current work in fabricating HBAR devices using aluminum nitride (AlN) as the piezoelectric and characterize the performance of our device, which uses a 2 µm film of AlN. With our AlN HBAR device, we find resonance modes from 300 MHz to 3.5 GHz with quality factors ranging from 800 to 1700.

Summary of Research:

The diamond NV-center consists of vacancy in the diamond lattice that is adjacent to a substitutional nitrogen. The goal of our research is the manipulation of the spin states of NV center through strain. Strain is introduced into the diamond lattice with piezoelectric transducers, such as high-overtone bulk acoustic resonators (HBAR). Examples of previous work with HBAR devices and diamond include coupling of the NV center spins with strain [1], coherent control over magnetically forbidden transitions of NV centers [2], continuous dynamical decoupling [3], and cooling of a mechanical resonator with a high-density NV ensemble [4].

In our current work at CNF, we are working on process development of HBARs that use AlN as the piezoelectric film with the aim of applying these resonators for control of NV spins for quantum metrology applications such as angle sensing [5]. Previously, we would have to have to AlN film deposited externally from CNF, but with the recent addition of the OEM Endeavor M1 tool, we are able to do the entire fabrication in-house.

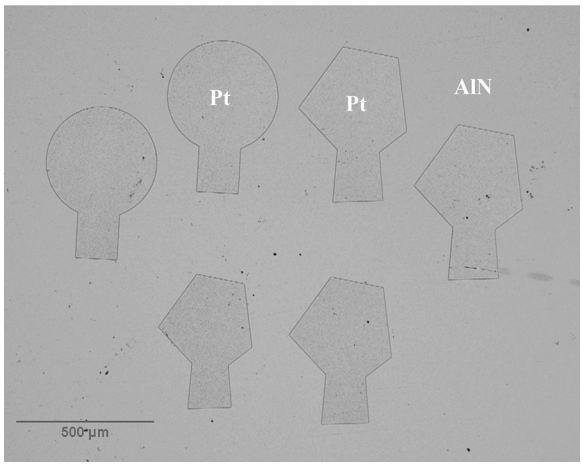

Figure 1: Final HBAR devices on the optical-grade diamond substrate. The devices are approximately 500 µm large. The top electrode, which defines the HBAR, consists of a Ti/Pt film and made through lift-off. These electrodes sit on the AlN layer which is 2 µm thick.

We fabricate these HBAR devices using AlN as the piezoelectric layer through the following process. The substrate that we work with is a 3 mm by 3 mm diamond piece. On top of the substrate, we sputter a layer of Ti/Pt (103 nm total thickness) to act as the bottom electrode of the device using the AJA sputter deposition tool at CNF. Following this, we sputter the piezoelectric layer of AlN (2 µm) using the OEM Endeavor M1 tool. To finish the fabrication, we define the shape of the top electrode though photolithography with the 5X stepper and sputter a Ti/Pt film (10nm/180nm) again with the AJA sputter deposition. The excess metal film on the top layer is

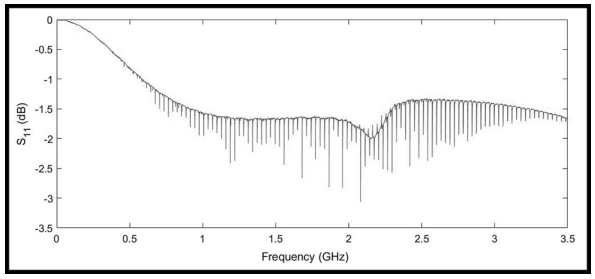

Figure 2: S11 measurement of the AlN HBAR device fabricated on optical-grade diamond. HBAR resonances modes are present in the S11 measurement in a frequency range of approximately 500 MHz to 3.5 GHz.

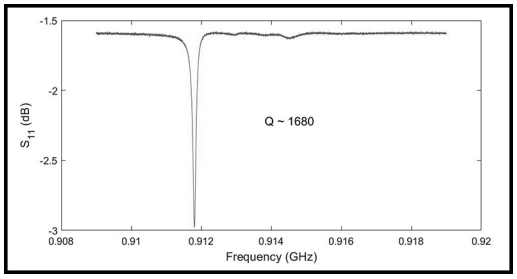

Figure 3: VNA Measurement single resonance mode of AlN HBAR device fabricated on optical-grade diamond. The quality factor that is extracted from fitting to Q-circle model is approximately 1680.

removed through lift-off, leaving behind the top electrode on the piezoelectric layer. In Figure 1, we see the final HBAR devices that are fabricated on diamond. These devices are approximately 500 μm large.

We tested the electromechanical response of our HBAR device with a vector network analyzer. The devices presented here are fabricated on optical-grade diamond, with a thickness of 287 μm and a variation of approximately 1 μm across 3 mm. Minimizing the thickness variation of the substrate is important for these devices as the top and bottom surfaces of the substrate act as planar mirrors for the stress wave injected into the substrate by the HBAR. The planar surfaces allow for an acoustic standing wave in the substrate. Having a large thickness variation is detrimental to the quality factor of our resonator. Using the vector network analyzer, we looked at the S11 response of our HBAR device. When the HBAR is resonant with the applied power, less power is reflected, which is seen as a dip in the S11 measurement. As seen in Figure 2, from the S11 measurement, we find that the resonance modes of our device span from 500 MHz to 3.5 GHz, with quality factors in the range of 800 to 1700. In Figure 3, we see a resonance mode with a quality factor of 1680 which was extracted using the Q-circle method [6].

Further work in being done to improve the performance and the consistency of these devices and to optimize the fabrication process. For example, the quality of the AlN piezoelectric layer limits the quality of the device. In our current process, we use a TMAH developer to define the top electrode area. However, TMAH etches the surface of the AlN film, increasing the surface roughness of the film, which lowers the performance of the device.

References:

[1] E. R. MacQuarrie, T. A. Gosavi, N. R. Jungwirth, S. A. Bhave, and G. D. Fuchs, Mechanical spin control of nitrogen-vacancy centers in diamond, Phys. Rev. Lett. 111, 227602 (2013).

[2] E. R. MacQuarrie, T. A. Gosavi, A. M. Moehle, N. R. Jungwirth, S. A. Bhave, and G. D. Fuchs, Coherent control of a nitrogen-vacancy center spin ensemble with a diamond mechanical resonator, Optica 2, 233 (2015).

[3] E. R. MacQuarrie, T. A. Gosavi, S. A. Bhave, and G. D. Fuchs, Continuous dynamical decoupling of a single diamond nitrogen-vacancy center spin with a mechanical resonator, Phys. Rev. B 92, 224419 (2015).

[4] E.R. MacQuarrie, M. Otten, S.K. Gray, and G.D. Fuchs, Cooling a mechanical resonator with nitrogen-vacancy centres using a room temperature excited state spin-strain interaction Nature Communications 8, 14358 (2017).

[5] Ashok Ajoy and Paola Cappellaro. Stable three-axis nuclear gyroscope in diamond, Phys. Rev. A 86, 062104 (2012).

[6] D. A. Feld, R. Parker, R. Ruby, P. Bradley, and S. Dong, in IEEE International Ultrasonics Symposium (IUS), Beijing, 2008 (IEEE, Piscataway, NJ, 2008), p. 431.

NanoThermoMechanical Logic Thermal Gates

CNF Project Number: 2357-15

Principal Investigator(s): Sidy Ndao

User(s): Ahmed Hamed

Affiliation(s): Mechanical and Materials Engineering, University of Nebraska-Lincoln

Primary Source(s) of Research Funding: This work was supported by the National Science Foundation (NSF) through the Nebraska Materials Research Science and Engineering Center (MRSEC) (grant No. DMR-1420645). This work was performed in part at the Cornell NanoScale Science & Technology Facility (CNF), a member of the National Nanotechnology Coordinated Infrastructure (NNCI), which is supported by the National Science Foundation (Grant NNCI-1542081)

Contact: sndao2@unl.edu, a.hamed@huskers.unl.edu

Primary CNF Tools Used: Heidelberg mask writer DWL2000, ASML 300C DUV, e-beam SC4500 odd evaporator, Oxford PECVD, Oxford 81 etcher, Unaxis 770 etcher, Tencor P7 profilometer

Abstract:

Today's electronics cannot perform in harsh environments (e.g., elevated temperature and ionizing radiation environments) found in many engineering applications. Thermal computing, data processing based on heat instead of electricity, is proposed as a practical solution and opens a new scientific area at the interface between thermal and computational sciences. We designed and modeled thermal AND, OR and NOT logic gates, achieved through the coupling between near-field thermal radiation (NFTR) and MEMS thermal actuation [1]. In the process, we also developed two novel non-linear thermal expansion designs of microstructured chevron beams. Using in-cleanroom standard microfabrication techniques in CNF, we successfully fabricated the designed thermal AND and OR gates.

Summary of Research:

Due to the success and feasibility shown by modeling the designed thermal gates, we were interested in fabricating and characterizing the proposed micro-structured thermal logic gates. In general, the microdevices that intended to be fabricated consist of chevron beams hold suspended plates, all are thermally actuated by platinum microheaters above the silicon microstructures. So, we designed three photolithography masks: platinum microheaters, silicon front side microstructures, and silicon backside etching. The microdevices are fabricated using in-cleanroom standard microfabrication techniques in CNF starting with a four-inch-diameter <100> silicon-over-insulator (SOI) wafer. The SOI wafer consists of a 400 µm thick handle silicon substrate, a 1 µm thick buried silicon dioxide layer, and a 20 µm thick boron-doped silicon device layer.

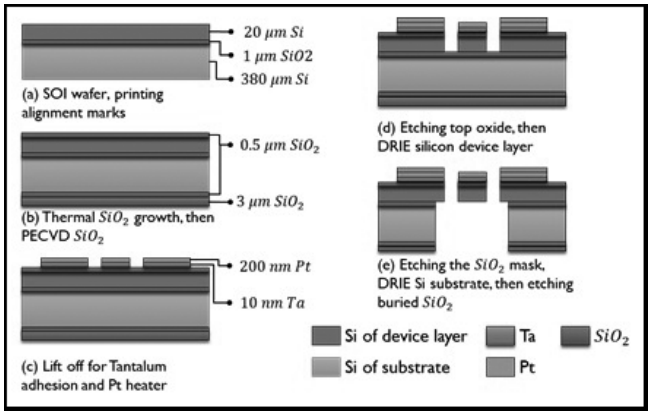

Figure 1: Fabrication steps of the two novel thermal expansion mechanisms (the reducing and the amplification mechanisms).

Figure 1 shows the steps followed through the microfabrication process flow adopted for the thermal gates' fabrication. Following a cleaning step of the wafers, a 0.5 µm thick silicon dioxide film (acts as an electrical insulator) is thermally grown by wet oxidation in a furnace at 1100°C (Figure 1b) on both sides of the wafer. On the substrate's backside, an additional 3 µm thick film of silicon dioxide is deposited via plasma enhanced chemical vapor deposition (tool: Oxford PECVD) to serve as an etching mask in subsequent backside etch steps. The microheaters (200 nm thick platinum and 10 nm thick tantalum as adhesion layer) are formed on top of the device layer using lift-off and e-beam evaporation (tool: SC4500 odd evaporator) as shown in Figure 1c. Following the formation of the microheaters, the suspended structures of the NanoThermoMechanical

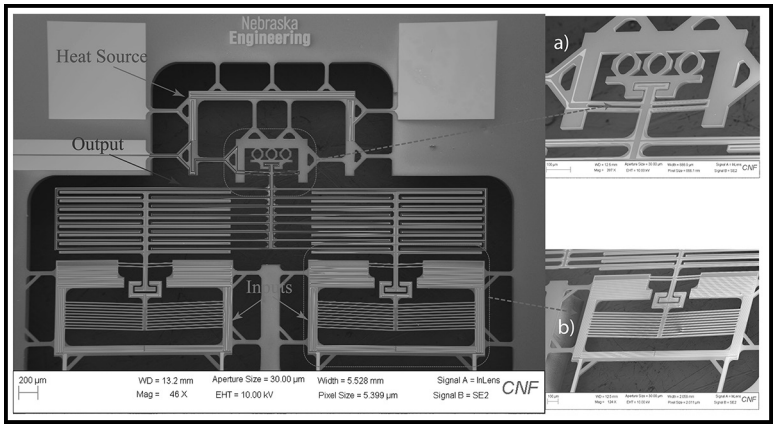

Figure 2: SEM images of the micro-structured thermal logic AND gate including: a) the reducing and b) the amplification mechanism.

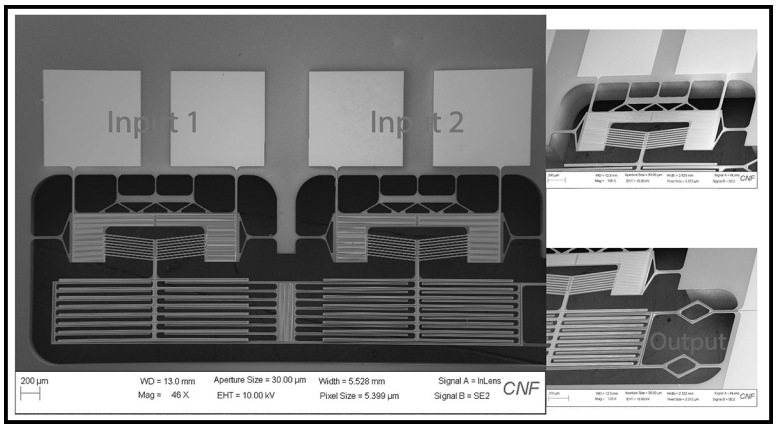

Figure 3: SEM images of the micro-structured thermal logic OR gate including two inputs (chevron beams) and output (fixed terminals).

gate (Figure 1d) were formed through steps of reactive ion etching (tool: Oxford 81 etcher) (to remove the 0.5 µm thick thermal silicon dioxide layer) and deep reactive ion etching of the silicon device layer (tool: Uniaxis 770 etcher). To release the final structures, backside etching (Figure 1e) on the silicon dioxide (tool: Oxford 81 etcher), silicon handle wafer (tool: Uniaxis 770 etcher), and buried oxide were performed (tool: Oxford 81 etcher).

We designed three photolithography masks (Heidelberg mask writer DWL2000): platinum microheaters, silicon front side microstructures, and silicon backside etching. These masks are employed through the microfabrication process flow adopted to fabricate the designed thermal gates. Figures 2 and 3 show the successful micro-fabrication of the thermal AND and OR gates, respectively, including the reducing and the amplification mechanisms for the thermal AND gate.

References:

[1] A. Hamed, M. Elzouka and S. Ndao, "Thermal calculator," International Journal of Heat and Mass Transfer, vol. 134, pp. 359-365, 2019.

Making a Microfluidic Device to Mimic Flow Through Porous Medium

CNF Project Number: 2385-15
Principal Investigator(s): Brian J. Kirby
User(s): Katherine Polhemus

Affiliation(s): Mechanical and Aerospace Engineering, Cornell University
Primary Source(s) of Research Funding: IGERT Program for Earth Energy
Contact: kirby@cornell.edu, kcp44@cornell.edu
Primary CNF Tools Used: Photolithography tools, hot press, deep reactive ion etcher, CorSolutions

Abstract:

With the rapid depletion of known oil reserves, detecting properties of the oil reservoirs and optimizing oil extraction is critical. By measuring the aqueous properties of the reservoirs, decisions can be made on which reservoirs to drill and the available quantity of oil to extract, with minimal environmental impact. Utilizing hairy nanoparticles in testing can provide a variety of information about the reservoir. The objective of the proposed work is to characterize the behavior of hairy nanoparticles at the oil-water interface in order to optimize their use as subsurface sensors. In order to complete the optimization, a microfluidic model for the environment needs to be developed. This past year's work involves making microfluidic devices to mimic water flowing through the subsurface and oil trapped in pores. The design and mold to make the mold was developed in the CNF first using photolithography to create a mold with negative photoresist which was used to make microfluidic channels out of polydimethylsiloxane and later using positive photoresist and etching to create a mold to make microfluidic channels out of polypropylene.

Summary of Research:

This work in the CNF has consisted of using microfabrication techniques to make a microfluidic device. Using the cad software L-Edit, we make patterns to transfer to a mask using the Heidelberg mask writer. In the past year, we have made two types of masks: one for positive photoresist and the other for negative photoresist.

The first set of microfluidic devices made used the negative photoresist (SU-8) to make a mold. The process of making a mold with photoresist (photolithography) consist of the steps: 1) pour and spin photoresist onto a wafer (using CNF spinner), 2) bake photoresist (using CNF hot plates), 3) wait time, 4) expose photoresist (using ABM contact aligner), 5) second wait time, and 6) development of photoresist. At the end of the process, we have a mold out of SU-8 on top of a wafer. In our research group's lab, we made microfluidic devices by pouring PDMS on top of the mold and baking then attaching the molded PDMS to a glass slide through plasma cleaning.

Unfortunately for this application, we need the PDMS to be very hydrophobic and PDMS was not hydrophobic enough for our experiments. Therefore, we switched to making devices out of a polypropylene — a much more hydrophobic material. To make molded polypropylene pieces we used hot embossing, which is done on the CNF hot press. Because of the large pressure applied during embossing, we needed a stronger mold than SU-8, so we switched to making molds out of silicon. To make a mold out of silicon, a positive photoresist is spun instead of negative and after the photolithography process, the wafer is etched on the Deep Reactive Ion etcher in the CNF. The mold is used in the CNF Hot Press to hot emboss the pattern onto polypropylene. Another piece of polypropylene is pressed to a thinner thickness using the using the hot press. Finally, the device is bonded together using the hot press.

We also used the CorSolutions as a connection method for tubes to the device, which allows us to flow oil and particles into the device.

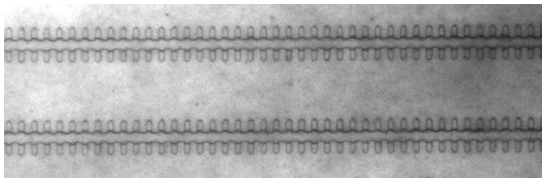

Figure 1: Oil-water contact line in polypropylene device.

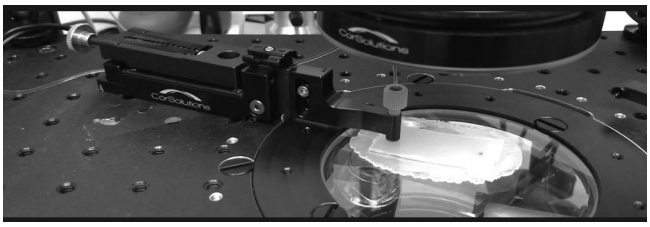

Figure 2: Device on CorSolution station.

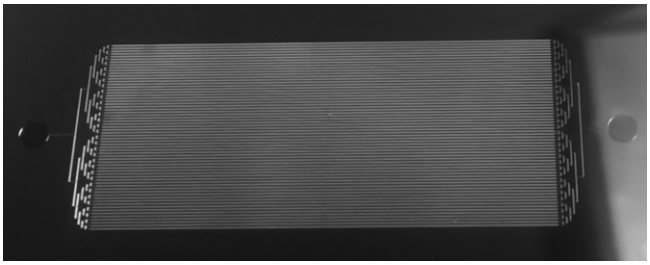

Figure 3: Etched silicon mold for hot pressing.

Atomically Thin Metamaterial Robots, Origami, and Artificial Flagella

CNF Project Number: 2416-16

Principal Investigator(s): Itai Cohen, Paul L. McEuen

User(s): Qingkun Liu, Baris Bircan, Wei Wang, Tianyu Ma

Affiliation(s): Kavli Institute at Cornell for Nanoscale Science, School of Applied and Engineering Physics, Laboratory of Atomic and Solid-State Physics, Department of Physics; Cornell University

Primary Source(s) of Research Funding: National Science Foundation, Contract: DMR-1719875; DMR-1435829 Army Research Office, Contract: W911NF-18-1-0032

Contact: itai.cohen@cornell.edu, plm23@cornell.edu, ql59@cornell.edu, bb625@cornell.edu, ww459@cornell.edu, tm478@cornell.edu

Primary CNF Tools Used: Oxford ALD FlexAL, Arradiance ALD Gemstar-6, Oxford 81 etcher, Oxford 100 etcher, ABM contact aligner, SC 4500 odd-hour, AJA sputter, AJA ion mill, Oxford Cobra ICP etcher, Heidelberg DWL2000

Abstract:

The ability to actuate an object at the microscale is an important technological aspect of manufacturing micro-robots and micro-machines. Here we demonstrate that micro-actuators made by atomically thin layers of metals and dielectrics could bend in response to electrical or chemical signals. These actuators could be designed into bidirectional bending modes, enabling chemically responsive micro-scale complex origami structures. By harnessing the electrical controllability and bidirectional folding structures, a mechanical metamaterial microrobot has been fabricated, allowing remotely controllable robotic sheets with large degree of freedom of motion.

Summary of Research:

Using commercial semiconductor processing techniques, our team has developed methods to deposit and pattern atomically thin films that can bend in response to chemical and electrical stimuli. This approach makes it possible to create complex structures, machines, and microrobots by using origami design principles at the microscale.

Our team first demonstrated an electrically responsive micro cantilever with an ultra small bending radii of 1-2 μm. The microcantilever has a bimorph structure comprising of 5 nm platinum (Pt) and 2 nm silica (SiO_2), both of which are deposited by atomic layer deposition (ALD). The exposed platinum surface expands at a low voltage of -0.2V in a buffer solution due to the hydronium (H_3O^+) adsorption on the platinum surface, bending the bimorph structure toward the silica layer. Based on this actuation mode of platinum/SiO_2 bimorph, we fabricated artificial flagella that could swing and drive the small particles to move in a buffer solution, as shown in Fig. 1.

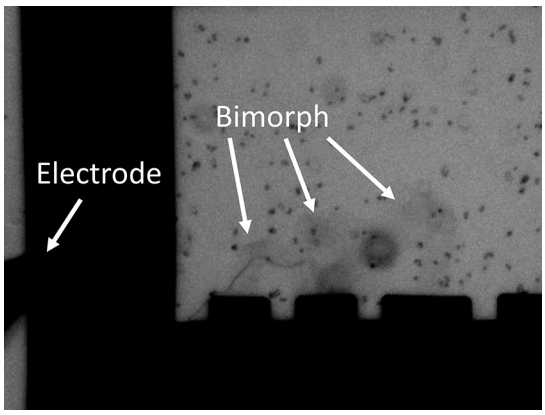

Figure 1: Electrically driven artificial flagella made by atomically thin Pt/SiO_2 bimorph structure swing in the buffer solution.

Our team has also demonstrated a technique to create micron scale folds using ultra-thin bending actuators composed of 2 nm of ALD grown SiO_2 and a sheet of monolayer graphene. These actuators are driven by ion exchange reactions, where larger H_3O^+ ions take the place of smaller Na^+ ions in the SiO_2 layer, causing swelling and creating a strain mismatch that produces unidirectional bending action.

Photolithographically defining fold patterns and localizing the bending using 1 μm thick panels of rigid SU-8 polymer enables the fabrication of elementary folded structures like cubes and tetrahedra [1].

Since origami design principles can be used to map any arbitrary shape to a crease pattern with fold angles ranging from -180° to +180°, bidirectional bending action is needed to create a complete platform for origami-based self-assembly at the microscale. The basic idea is that if one type of bimorph stack bends upwards, the order of the stack can be inverted to produce downward bending. To achieve this, our group has developed a method for growing and stitching together all ALD grown Si_3N_4-SiO_2 bimorph stacks. Replacing graphene with ALD Si_3N_4 not only makes the fabrication more easily scalable, but also eliminates the need for any additional functionalization step that would be required to perform ALD on graphene. This strategy makes it possible to design and fabricate origami devices of variable complexity that can sense changes in pH and change configurations from flat to folded according to prescribed mountain-valley folds.

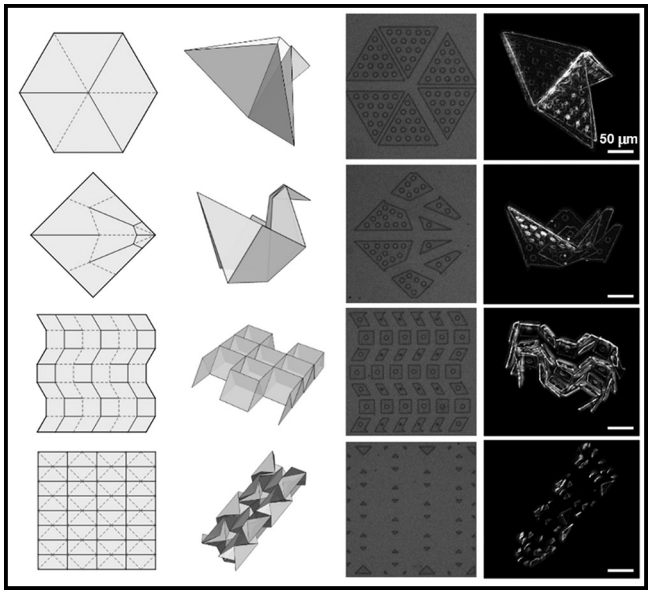

Figure 2: Origami designs of variable complexity constructed at the microscale using all-ALD bimorphs. Columns from left to right: Origami crease patterns, computer models of folded shapes, micro-origami devices (unfolded), micro-origami devices (folded). Scale bars are 50 µm.

Figure 2 shows a variety of origami designs fabricated using this method, ranging from relatively simple ones with six folds to more complex structures with more than 100 folds. The origami bird made using our approach is less than half the size of the current state of the art [2]. Having established a complete platform for micro-origami with ion exchange actuated bimorphs, our group is preparing to develop bimorphs consisting of atomic layer deposition Pt and SiO_2, which will make it possible for us to achieve bidirectional bending action through electrical actuation.

By harnessing the electrical controllability and bidirectional folding structure, our team designed and fabricated

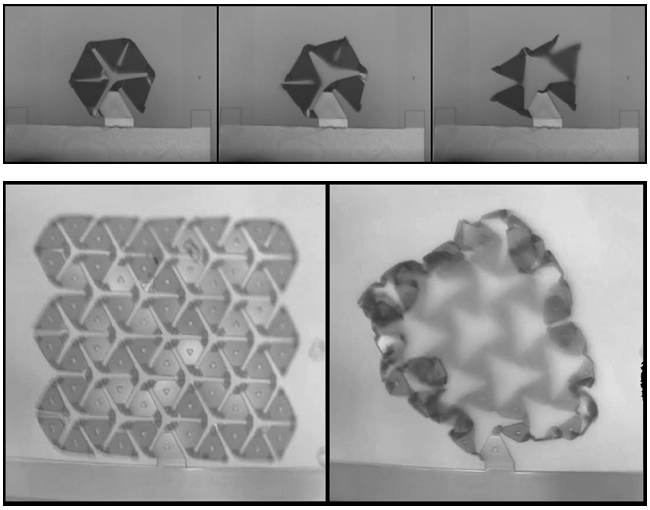

Figure 3, top: Three images from a movie showing voltage-based actuation of nm thin hinges of a six-panel metamaterial sheet.

Figure 4, bottom: A flat mechanical metamaterial microrobotic sheet (left) shows expansion and wrapping modes (right).

metamaterial robots that could locally expand and change its Gaussian curvature. Once integrated with electronics, such robots will be able locomote, wrap, and encapsulate synthetic and biological materials. To generate local expansion of the metamaterial robot it is necessary to create hinges that allow panels to splay. The three folding actuators with opposite bending directions are connected to two panels. The middle hinge can bend at an angle of 180°, while the two side hinges can bend at an angle of 90° in the opposite direction.

Having determined that this design was mechanically feasible, we fabricated, using alternating layers of ALD grown Pt and sputtered Ti that are 7 nm thin, the first bidirectional surface electrochemical actuators. We used these voltage-driven actuators to implement a proof or principle scaffold for the metamaterial robot (Figure 3). Integrating these building blocks into a sheet structure, we fabricated mechanical metamaterial-based microrobots with large degree of freedom (Figure 4). This sheet-like microrobot could expand into three-dimensional structure, wrap the target object and shrink its size, opening the door to diverse applications in medical treatment and drug delivery.

References:

[1] Miskin, M., Dorsey, K., Bircan, B., Han, Y., Muller, D., McEuen, P., and Cohen, I. Graphene-based bimorphs for micron-sized autonomous origami machines. Proceedings of the National Academy of Sciences, 115: 466-470 (2018).

[2] Bircan, B., Miskin, M., Dorsey, K., McEuen, P. and Cohen, I., Bidirectional Folding with Nanoscale Sheets for Autonomous Micro-Origami, 2018.

A MEMS Microphone Using Levitation Force

CNF Project Number: 2446-16

Principal Investigator(s): Shahrzad Towfighian, Ronald N. Miles

User(s): Mehmet Ozdogan

Affiliation(s): Mechanical Engineering Department, State University of New York at Binghamton

Primary Source(s) of Research Funding: National Science Foundation Project ECCS grant # 1608692 titled "A new Approach to Capacitive Sensing: Repulsive Sensors"

Contact: stowfigh@binghamton.edu, rmiles@binghamton.edu, mozdoga1@binghamton.edu

Website: https://www.binghamton.edu/labs/mems/

Primary CNF Tools Used: LPCVD N+/P+ Polysilicon-Wet Oxide-CMOS Nitride, MOS clean anneal, Heidelberg mask writer DWL2000, AS200 i-line stepper, Plasma-Therm deep Si etcher, Oxford 80+-100 etchers, Oxford PECVD, Zeiss Ultra SEM, dicing saw, Leica critical point dryer

Abstract:

We report fabrication and preliminary experimental results of a microelectromechanical systems (MEMS) microphone using a levitation force-based electrode configuration. This electrode scheme causes the sensing electrode (attached to a diaphragm) to move away from the biasing electrode as DC source is applied. The devices employing this scheme benefit from pull-in free behavior. Main objective of this work is to fabricate a MEMS microphone whose sensitivity could be improved simply by increasing the bias voltage, without suffering from pull-in instability. The microphone was fabricated at CNF and tested in Binghamton University anechoic chamber. The output of the chip at various bias voltages are measured using a read-out circuit. Experimental results show that the sensitivity of the device increases with increasing bias voltages from 40 volts to 100 volts. The ability to design electrostatic sensors without concerns about pull-in failure can enable a wide range of promising sensor designs.

Summary of Research:

A microphone is an acoustic sensor that converts mechanical motions generated by sound pressure waves into electrical signals. Every year, billions of MEMS microphones have been produced and integrated into consumer products such as smartphones, laptops, hearing aids, smart wireless speakers etc. The sensitivity of the microphone is one of the most important parameters that defines the quality of a microphone. In general, the sensitivity is proportional to the applied bias voltage. However, usual electrode configurations (one fixed and one moving electrode) mostly suffer from pull-in instability, which causes the device stop functioning after some certain DC bias values. The levitation (repulsive) electrode configuration has been widely investigated and shown to be pull-in safe [1-3], which enables MEMS devices to have large travel ranges and proper functioning at high DC loads. This method utilizes fringe electrostatic field to generate a net force that pushes the diaphragm away from the substrate which eliminates the pull-in possibility. The microphone design consists of fixed and moving electrodes which are attached to a rotating diaphragm, see Figure 1. The design includes three sets of electrodes: grounded sensing electrodes, grounded fixed electrodes and biasing electrodes. The moving and fixed electrodes are vertically separated.

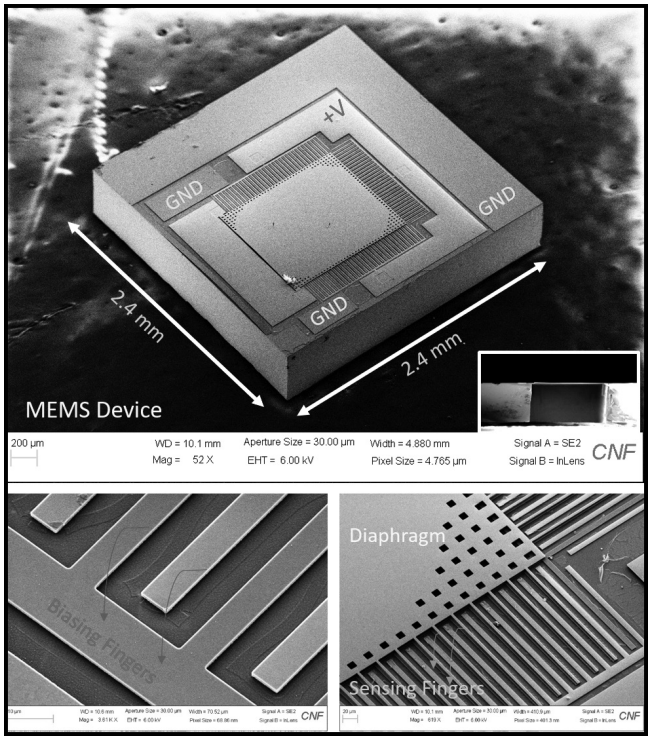

Figure 1: Images of the fabricated device. (Top) SEM image of the microphone and the cross section of the released chip. (Bottom Left) Biasing fixed fingers. (Bottom Right) Moving Finger and the diaphragm.

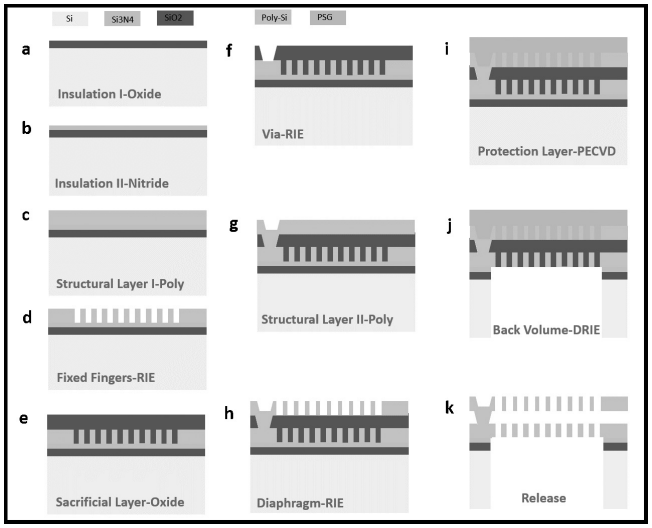

Figure 2: Fabrication process flow of the sensor.

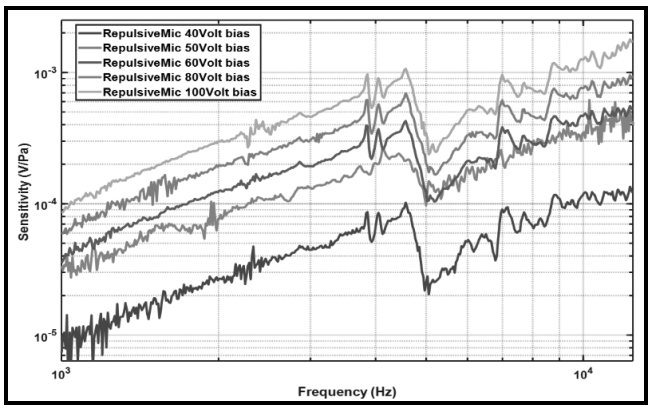

Figure 3: Experimental results. Shows the change of sensitivity of the microphone as the DC bias increases.

Process flow for the fabrication of the MEMS microphone is depicted in Figure 2. We started with 100 mm silicon wafers and grew 1 μm thick LPCVD silicon dioxide as an insulation layer. Following this step LPCVD low stress silicon nitride was deposited on top of the oxide layer. On top of the insulation layers 2 μm thick polysilicon layer was deposited and annealed using LPCVD furnace. This layer was etched using Unaxis 770 silicon etcher to form fixed fingers, Figure 3. On top of the fingers, 4 μm thick sacrificial layer of LPCVD high-temperature-oxide (HTO) was deposited. Then, Logitech Orbis chemical mechanical polisher (CMP) was used to remove half of the oxide layer which yielded around 2 μm vertical gap between fixed and moving electrodes. Then, Oxford 100 etcher is used to create vias on this sacrificial layer. Later, second 2 μm thick polysilicon layer was deposited and annealed to reduce the residual film stresses. This layer was etched to form the diaphragm and the sensing electrodes.

Next, we deposit phosphosilicate glass (PSG) using Oxford PECVD tool. This layer mechanically supported the diaphragm while etching the back-volume of the device. The back volume was created by etching the bulk silicon using Plasma-Therm deep silicon etcher. Then, wafers were diced into 2.4 mm by 2.4 mm chips, which are then released in HF:HCl mixture and critical-point-dried.

After the microphone was released the chip was glued on a printed-circuit-board (PCB) and wire-bonded. A charge amplifier-based read-out circuit was used to obtain electrical signals. The acoustic tests for the microphone were performed in the anechoic chamber at Binghamton University. We applied various DC voltages to the biasing electrodes. This DC voltage created an out-of-plane motion to the diaphragm and increased the initial gap between the diaphragm and the fixed electrodes. The sound pressure was created by a loudspeaker by sweeping a broad range of pure tone signals (100 Hz-20 Khz). The incident pressure measured using a Bruel&Kjaer 4138 reference microphone. The electronic output from the chip was detected using a charge amplifier read-out circuit. The circuit consisted of an operational, capacitors and feedback-resistors. The sensitivity plot was obtained by measuring the output voltage relative to the sound pressure. The signals were acquired using a National Instruments Data Acquisition System.

Figure 3 shows the measured electrical response of the microphone for a wide range of bias voltages. It is shown that levitation electrode concept improves the sensitivity of a MEMS microphone simply by increasing the DC bias voltage without any pull-in failure.

This approach can enable designs that employ large bias voltages without adversely impacting the diaphragm's mechanical response.

References:

[1] S. He and R. B. Mrad, "Design, Modeling, and Demonstration of a MEMS Repulsive-Force Out-of-Plane Electrostatic Micro Actuator," in Journal of Microelectromechanical Systems, vol. 17, no. 3, pp. 532-547, June 2008.

[2] Towfighian S, He S, Ben Mrad R. "A Low Voltage Electrostatic Micro Actuator for Large Out-of-Plane Displacement.", ASME. IDETC/CIe, Vol. 4: doi:10.1115/DETC2014-34283.

[3] Ozdogan M, Daeichin M, Ramini A, Towfighian S, "Parametric Resonance Of A Repulsive Force MEMS Electrostatic Mirror.", Sensors and Actuators A: Physical, Volume 265, 2017, Pages 20-31.

[4] Daeichin M, Ozdogan M, Towfighian S, Miles R, "Dynamic Response Of A Tunable MEMS Accelerometer Based On Repulsive Force.", Sensors and Actuators A: Physical, Volume 289, 2019, Pages 34-43.

Carbon Dioxide as Thermal Fluid in Micro Systems

CNF Project Number: 2474-16
Principal Investigator(s): Dr. Yoav Peles
User(s): Mostafa Asadzadeh, Anatoly Parahovnik

Affiliation(s): Mechanical and Aerospace Engineering, University of Central Florida (UCF)
Primary Source(s) of Research Funding: Office of Naval Research (ONR)
Contact: yoav.peles@ucf.edu, asadzade@knights.ucf.edu, tolik@knights.ucf.edu
Primary CNF Tools Used: AJA sputter deposition, chemical mechanical polishing (CMP)

Summary:

Carbon dioxide (CO_2) is a natural coolant that present an alternative for environmentally hazardous coolants like hydrocarbons. The highest potential of CO_2 is in the trans critical region where it's thermophysical properties exhibit largest variations. For example, CO_2 viscosity lowers significantly during transition from liquid to supercritical phase, such reduction enables to reduce the pressure drop inside a micro channel and to achieve higher mass fluxes leading to a better heat removal. The project goal is to fabricate a microfluidic device that will enable to better understand thermal behavior of CO_2 in the vicinity of the critical point — a temperature and pressure of 31.4°C and of 7.37 MPa, respectively. This requires the microfluidic device to function under high pressure.

The part that was fabricated at CNF is shown in Figure 1. It has heaters and resistor temperature detectors (RTDs) depicted as the white and brown layer, respectively. These layers were deposited using AJA sputter deposition tool, and then separated and sealed using silicon oxide that was applied using plasma enhanced chemical vapor deposition (PECVD).

To achieve good sealing of the microdevice, the top surface was polished using chemical-mechanical polishing process. The wafer was then placed in a DISCO dicing saw to separate the devices. With the AJA sputter tool and the help of the CNF staff we were able to achieve very high repeatability in respect to electrical resistance. To minimize fluid leakage, the top surface was polished to an average roughness of 150 nm. This helped ensure a leakage of several orders of magnitude smaller that the intended mass flow inside the device.

Figure 2 presents the microdevice assembly where the bottom substrate has the control components (i.e., the heaters and the RTDs) and the top substrate has the microchannel. The top substrate is made of fused silica to allow optical access to the microchannel.

Figure 3 presents an image of flow patterns at different phases — gas, liquid, and supercritical. The applied heat flux is 17 W/cm^2, the inlet temperature is 23°C, and the mass flux is 500 kg/m^{2}s for all images. The pressures are 5.34 MPa, 6.6 MPa and 8 MPa for gas, liquid and supercritical respectively. For the liquid phase there is formation of bubbles inside the channel which corresponds to heat removal by boiling. Bubble inside pressure is inversely proportional to its diameter,

Therefore, due to high operating pressure the bubbles are small. In the images of the gas and supercritical phases, vertical lines can be seen. The lines correspond to equal density, which are dependent on the refraction index, and therefore visible using the camera. For the supercritical phase the lines are more distinct corresponding to larger variation of the density due to local heating. These density variations promote mixing, and therefore, enhance the heat transfer at the supercritical phase. It was found that the heat transfer coefficient of supercritical phase was enhanced by approximately 20% compared to the gas phase.

Our future work includes further investigation of heat transfer patterns at the trans-critical region. Gaining better understanding of the mechanisms controlling the heat transfer process will enable to have more efficient thermal control in microsystems.

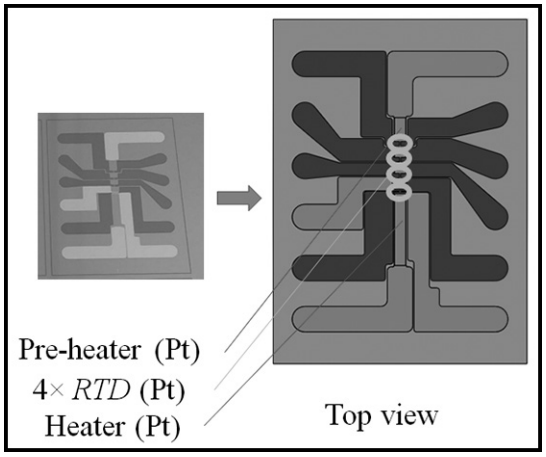

Figure 1: The microfabricated piece.

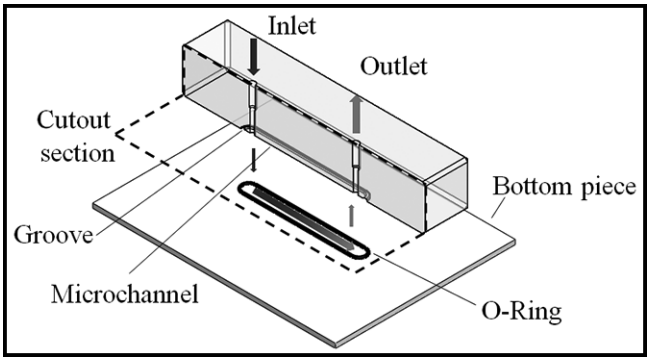

Figure 2: Microdevice assembly.

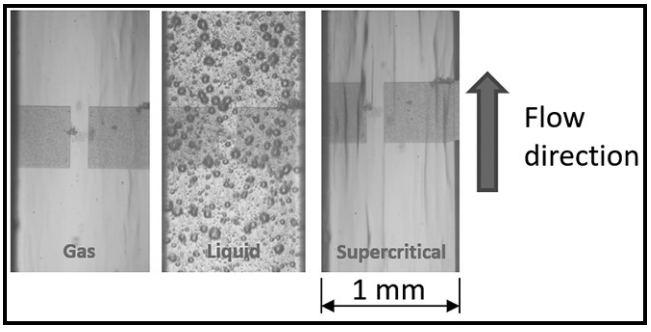

Figure 3: Heat transfer patterns at for different phases of CO_2.

Fabricating Vitreous Silica Micropillars for Uniaxial Compression with *in situ* Raman Spectroscopy

CNF Project Number: 2632-18

Principal Investigator(s): Shefford Baker

User(s): Zachary Rouse

Affiliation(s): Materials Science and Engineering Department, Cornell University

Primary Source(s) of Research Funding: Corning, Inc.

Contact: spb14@cornell.edu, zwr6@cornell.edu

Website: https://baker.mse.cornell.edu/

Primary CNF Tools Used: Autostep i-line stepper, PT770 etcher, Oxford 100 etcher, Oxford 81 etcher

Abstract:

In silicate glasses, the interplay between glass structure and plastic deformation is not well understood. To address this, high-quality SiO_2 micropillars were fabricated through a reactive-ion etching based method which were then tested in compression while characterizing the structure of the glass *in situ* using Raman spectroscopy. These experiments provide direct observation of how the structure of the glass changes in response to a well-known uniaxial stress and strain state. The SiO_2 micropillar fabrication process, as well as considerations for optimizing pillar geometry are described.

Summary of Research:

Silicate glass is a vital component in countless applications such as display screens, solar panels, and vehicle windshields and as such its fabrication has become a near trillion-dollar industry. Although silicate glasses are macroscopically brittle materials, in small volumes they can undergo extensive plastic deformation. The character of this deformation influences the stress field evolution and crack nucleation around mechanical contacts, ultimately dictating the bulk fracture of the glass. Despite this, very little is known about the underlying atomistic mechanisms leading to silicate glass plasticity.

A popular method of probing these mechanisms is to perform Raman spectroscopy of residual indentations *ex situ*. A basic understanding of how the glass network reconfigures during deformation can be acquired by associating spectral peaks with known glass network features and then observing the spectral shifts between a pristine and an indented region. However, the quantitative analysis of data acquired through this method is limited due to the poorly known and highly heterogeneous stress/strain states of the probed volumes underneath the indentations. Additionally, these *ex situ* tests only characterize the nature of the glass network due to residual deformation, rather than during deformation. To rectify this, we developed a novel experimental method in which Raman spectra are recorded *in situ* during uniaxial micropillar compression of SiO_2.

This testing enables us to probe the structure of a glass that is being subjected to well-known, homogeneous, and easily tunable stress and strain-states.

The success or failure of this method is entirely dependent on the ability to fabricate numerous high-quality SiO_2 micropillars with highly vertical side walls and minimal structural damage. To accomplish this, a new reactive-ion etching based process was developed at CNF. In this process first a thick (> 1.25 μm) chromium film is sputtered onto a standard SiO_2 wafer using the CVC 601 sputtering tool. An anti-reflective coating (ARC) followed by photoresist is then spun coat on top of the chromium. A reticle with a grid of circles with various diameters is then used for the resist exposure on the Autostep 200 stepper tool. After development (and oxygen plasma etching of the uncovered ARC), the residual discs of resist are used as a mask for a chlorine-based reactive-ion etch through the chromium film in the Plasma-Therm 770 etcher. After removal of the remaining resist, the residual discs of chromium are used as a mask for an extremely deep (6-10 μm) fluorine-based reactive-ion etch of the underlying SiO_2 wafer on the Oxford 100 etcher. The remaining chromium caps are dissolved with a chemical chromium etchant, and the passivating fluropolymer layer left on the pillar sidewalls is stripped with an EKC solvent.

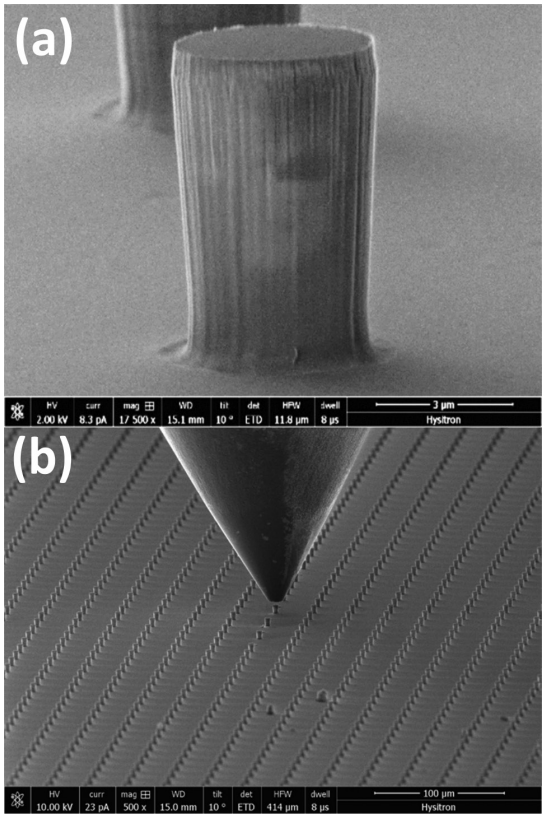

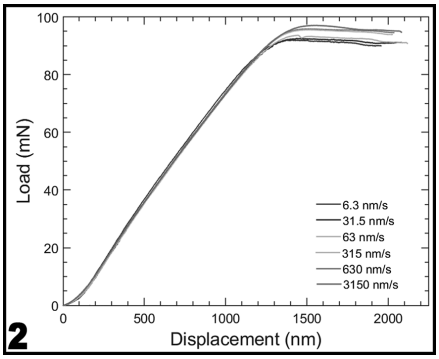

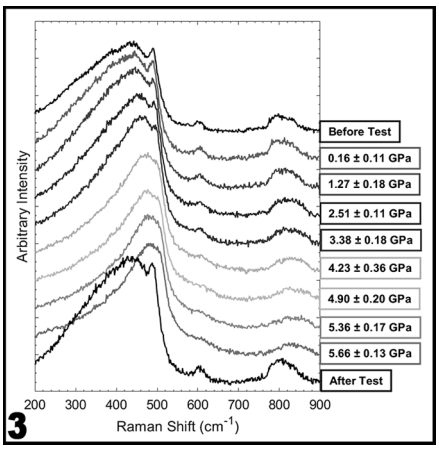

Figure 1, above: left (a) Scanning electron images of one typical silica micropillar and (b) a wide view of an array of micropillars as well as the diamond flat punch used to compress them. Figure 2, top right: Schematic of the utilized testing setup for micropillar compression with in situ *Raman spectroscopy. Figure 3, bottom right:* Ex situ *and* in situ *Raman spectra taken during micropillar compression at various applied engineering stresses. Spectrum peaks are associated with specific, known SiO_2 network features.*

This process leads to the creation of millions of pristine SiO_2 micropillars such as the one shown in Figure 1. Other SiO_2 micropillar compression studies made through analogous fabrication procedures have struggled with highly uneven pillar cross-sections [1,2]. This study's pillars are extremely dimensionally uniform and have only a slight negative taper angle of 1.8°. The tapering observed in other studies is largely caused by slanted side walls in the initial photoresist side walls, which transmits into the chromium (and then later into the SiO_2) when the resist is used as a mask. To mitigate this, a stepper exposure tool (as opposed to a contact exposure tool) using carefully optimized exposure parameters was used. During the etching stages, obtaining a very high etch selectivity was also critical for mitigating the transmission of a taper from the masks to the substrates.

To compress these pillars, the wafers were cleaved into pieces which were then mounted on a nanoindenter system (Bruker) equipped with a diamond flat punch tip. The nanoindenter system was then incorporated into a confocal Raman microscope (Renishaw InVia) such that micropillars near the cleaved edges could be probed by the Raman laser while simultaneously being compressed by the indenter punch as shown in Figure 2. By repeatedly raising the applied stress and then pausing to acquire a Raman spectrum, we can observe *in situ* Raman spectra as a function of a well-known uniaxial stress and strain for the first time ever (Figure 3).

From the dramatic peak shifts in these Raman spectra we can see that significant structural rearrangements occur with increasing applied stress, but surprisingly it is also observed that a large portion of these structural changes recover upon unloading of the pillar. This provides strong evidence that elastic deformation in SiO_2 significantly alters the glass network structure and provides a physical justification for silica's highly non-linear elastic behavior. By connecting the observed Raman peaks with SiO_2 network features, future quantitative analysis of these spectra will enable us to illuminate the fundamental atomic mechanisms of silicate glass deformation in a way that has never been possible before.

References:

[1] Kermouche, G., et al. (2016). "Perfectly plastic flow in silica glass." Acta Materialia 114: 146-153.

[2] Lacroix, R., et al. (2012). "Plastic deformation and residual stresses in amorphous silica pillars under uniaxial loading." Acta Materialia 60(15): 5555-5566.

Construction of Microplasma Test Array

CNF Project Number: 2762-19
Principal Investigator and User(s): Andrew Dickens
Affiliation(s): WildSpark Technologies LLC

Primary Source(s) of Research Funding: U.S. Department of Defense
Contact: andrew.dickens@wildsparktech.com
Website: WildSparkTech.com
Primary CNF Tools Used: ASML 300C gamma coat / develop tool, SC4500 deposition

Abstract:

Since 2016, WildSpark Technologies LLC has been working to develop and commercialize microplasma devices. Microplasma devices create and manipulate small regions of plasma from gas, solid, or liquid feedstock. These devices show promise for novel applications in electron devices, displays, medical devices, and flow control. Our lean and agile team uses the resources at the CNF to rapidly test concepts and construct prototype devices for test. In this report we discuss our efforts to build a system of electrodes and substrate stack to probe material and physical parameters which are used as building blocks for more complicated devices. The physical data extracted from these prototype devices is used to calibrate models used in multiphysics simulation to predict device performance in real world applications.

Summary of Research:

We created patterns of electrodes on varying substrate materials. These patterns formed microplasma actuator elements and were windowed across a range of dimensions and physical designs. We then tested the devices using semiconductor parameter analyzers and were able to directly measure — for the first time — our microplasma cells in action. Our company constructed several devices with different material stacks and substrate composition to assess the impact of material parameters on performance. The electrical test data was used in combination with physical simulation in order to isolate physical parameters, in particular the Fowler-Nordheim tunneling equation coefficients for the material system.

We were concerned about the ability of our test devices to operate under high power densities for a long period of time. The results of these experiments demonstrated an ability to operate at power densities exceeding $0.5W/mm^2$ for several minutes without degradation. This result exceeded our expectations and allows us to consider designs and power densities that we previously thought to be unattainable. While there are few comparable technologies in the literature, we believe this represents a milestone in terms of device endurance.

We chose CNF as a fabrication facility primarily because of the availability of the ASML 300C 248 nm stepper and gamma coat / develop system. Our work requires us to pattern very fine structures with tight tolerances for both critical dimension (CD) and registration. It is very difficult to find production 248 nm lithography tools available for use by small businesses and our work would not be possible without these tools.

We extensively used the SC4500 deposition tools in order to deposit titanium electrodes as well as some proprietary surface coatings to our electrode / substrate sandwiches. Interconnects and bond pads were constructed using a metal liftoff technique with aluminum deposition.

Our future work at CNF will include further refinements of our test arrays to gain new insight into microplasma device physics and eventually to produce prototype products based on this knowledge.

References:

[1] Arakoni, R, et al., "H_2 Generation in Ar/NH_3 Microdischarges", J Phys. D: Appl. Phys. 40 (2007) 2476-2490.

[2] Strong, F, et al., "Electrical discharge across micrometer-scale gaps for planar MEMS structures in air at atmospheric pressure", J. Micromech. Microeng. 18(2008) 075025, page 11.

[3] Nishida, Y, et al., "Hydrogen Production from Hydrocarbons With Use of Plasma Discharges Under High Pressure Condition", IEEE Transactions on Plasma Science, Vol 42, No 12, December 2014.